Supporting Material

Supplementary Methods

Tissue dissection and Immunohistochemistry

Wistar rats weighing 250 g were euthanised using by an intra-peritoneal injection of 100 mg per kg of body weight sodium pentabarbitone using a protocol approved by the University of Auckland Animal Ethics Committee. The extensor digitorum longus (EDL) and SOL muscles were dissected with intact tendons before pinning out immersed in standard Ringer's solution. The muscles were immediately fixed in 2% paraformaldehyde in phosphate buffered saline (PBS) for 1 hour at room temperature (21^{o}C). Fixed muscles were washed in fresh PBS for 10 minutes and cryoprotected in PBS containing 30% sucrose. They were frozen in methylbutane cooled in liquid nitrogen and sectioned into 10 µm thick cryosectioned at -25^{o}C using a CM 1900 cryostat (Leica, Germany). Sections were mounted onto number 1.5 glass coverslips coated with 0.05% poly-L-lysine (Sigma-Aldrich) and hydrated with PBS immediately. Hydrated sections were blocked in PBS containing 10% normal goat serum (Vector Laboratories Ltd, Burlingame, CA) for 10 minutes at room temperature before the incubating the primary antibodies in the antibody incubation buffer overnight at 4^{o}C. Coverslips and sections were rinsed in fresh PBS in three 20-min steps prior to the application of the secondary antibodies for 2 hours at room temperature. Three further rinsing steps were applied prior to immersing the sections in the imaging buffer and sealing the coverslips onto glass microscope slides.

dSTORM imaging

Slides containing the samples were clamped onto a stage driven by a piezo focuser (P-725, Physik Instrumente, Germany) on a modified Nikon TE2000 inverted total internal reflection fluorescence (TIRF) microscope. The laser beam from a solid-state 671 nm laser (Viasho, China) was focused onto the sample via a 60x 1.49NA oil-immersion TIRF objective (Nikon) in a highly inclined light sheet (1) to achieve a non-TIRF illumination of a 10 µm wide area up to several microns deep within the sample. Emission light was passed through a Q680LP dichroic mirror (Chroma Technology) and an XF3104-690ALP emission filter (Omega optical) prior to being split into two spectral channels using a custom-built splitter device built as described previously (2). During image acquisition in standard 2D dSTORM, the

focus was stepped repeatedly through a 1-1.5 μm z-range at 150 nm steps and the emission light in the two channels were recorded onto the two halves of the cooled EM-CCD chip of an IXon DV887DCS-BV camera (Andor Technology, Belfast) onto 30,000-40,000 frames at 20 frames/s.

dSTORM Image analysis

Single molecule events were localised and their spectrally separated into their fluorochrome identities using custom-written algorithms implemented in Python described previously (3). Greyscale images of each channel were rendered using a protocol based on Delaunay triangulation developed by Baddeley and others (4). Here, each detected event point was jittered randomly at an amplitude that was proportional to the average distance between this point and its nearest neighbour prior to the calculation of Delaunay triangulation. Averaging between ten independent triangulations produced a greyscale image at a pixel sampling of 5 nm/pixel with minimal background where intensity was proportional to the local event density.

To constrain the analysis to a single triad in the longitudinal plane (i.e. to avoid the projection of fluorophores from the triads of neibouring sarcomeres), only optical sections where RyR labelling densities are in focus were selected for analysis. Further, only transverse dSTORM images from fibres whose longitudinal axis aligned well with the optical axis of the microscope were considered for quantitative analysis. Among these images, only regions where the local plane of labelling (i.e. plane of the z-line, which may locally be observed as highly inclined angles relative to the transverse plane (5)) is no greater than ~5^{o} from the image plane were selected to ensure that the area of labelling observed broadly reports the footprint of the RyR arrays within the triads. Binarisation of regions containing positive labelling was performed by constructing Delaunay triangulation between all detected points in each channel and merging all triangles that were shorter than the effective resolution (typically 30 nm), while discarding any triangles longer than this limit (described previously; Baddeley and others (6)). See Supplementary Figure S1 for example. Binary and greyscale images were used for calculating the local density of RyRs. The maximum number of RyR footprints corresponding to this 2D binary area was calculated assuming an isotropic 30 nm centre-to-centre receptor packing density. This number was doubled (to reflect the two layers of receptors on either side of the triad) to obtain the local density of RyRs in receptors/μm^2.

To convert this into a concentration value (receptors per μm^2) this value was further divided by the axial depth of integration (1000 nm). The binary masks were also used for a co-localisation analysis according to a protocol described by Jayasinghe and others (7),(8). This analysis plotted histograms of the percentage integral of labelling of protein A as a function of the Euclidean distance to the edge of the nearest region of labelling of protein B (See Fig. 4C&F; 5F&I and S5). The shaded bars in these histograms illustrate the percentage of protein A determined to be co-localised within the mask of protein B. A summary of these co-localising fractions is shown in Table 2.

Solutions and antibodies

The Ringer solution used for dissolving the fluorescent dye solution contained 112 mM of NaCl (Sigma-Aldrich), 3.3 mM of KCl (Sigma-Aldrich), 2.5 mM of $CaCl_2$ (Sigma-Aldrich), 1 mM of $MgCl_2$ (Sigma-Aldrich) and 20 mM of Hepes (Sigma-Aldrich) with the pH adjusted to 7.4 using NaOH. Primary and secondary antibodies were incubated in PBS containing 0.05% NaN_3 (w/v), 2% bovine serum albumin (w/v), 2% normal goat serum (v/v) and 0.05% Triton X100 (v/v). The imaging buffer for localisation microscopy contained 90% Glycerol (v/v) and 5 mM β-mercaptoethylamine (Sigma-Aldrich) in PBS.

Primary antibodies used for immunohistochemistry were mouse monoclonal anti-RyR raised against partial RyR1 of chicken pectoral muscle ((9,10); MA3-925; Thermo Scientific), rabbit poly-clonal anti-junctophilin-1 (JPH1) C-terminus (40-5100; Zymed) and mid-region antibodies (40-5200; Zymed), a rabbit poly-clonal anti-Junctophilin-2 (JPH2) C-terminus antibody (40-5300; Zymed), a mouse monoclonal anti-calsequestrin (CSQ; MA3-913; Thermo Scientific) that recognises both CSQ1 and CSQ2 (11,12) and a mouse monoclonal anti-Triadin (Trdn; ab2870; Abcam). Alexa 680- and Alexa-750 conjugated highly cross-adsorbed (H+L) goat anti-mouse IgG and goat anti-rabbit IgG antibodies (Molecular Probes, Life Technologies) were used as secondary antibodies in these labelling experiments.

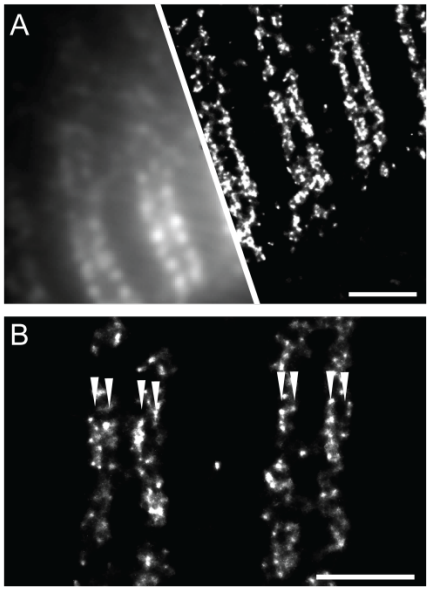

Figure S1. Super-resolution imaging of RyR immunolabelling of mammalian skeletal muscle. (A) A split-image comparison of an RyR-labelled fibre from a longitudinally sectioned EDL muscle in a diffraction-limited widefield image (left) and super-resolution dSTORM (right). (B) Magnified view of a longitudinal dSTORM image illustrating the double-row morphology (arrows) of RyR labelling at the expected A-I boundaries of the sarcomere. Scale bars: A: 2 µm, B: 1 µm.

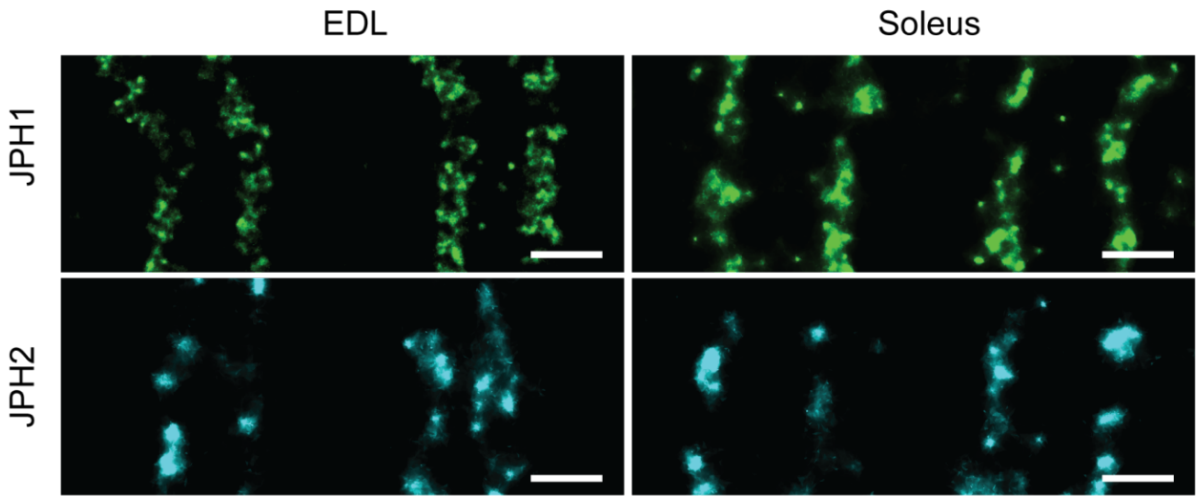

Figure S2: dSTORM images of JPH1 (green) and JPH2 (cyan) in longitudinal sections of adult rat EDL (left) and soleus (right) muscle. Note that JPH1 and JPH2 data were obtained in separate fibres due to antibody host species constraints. Scale bars: 500 nm.

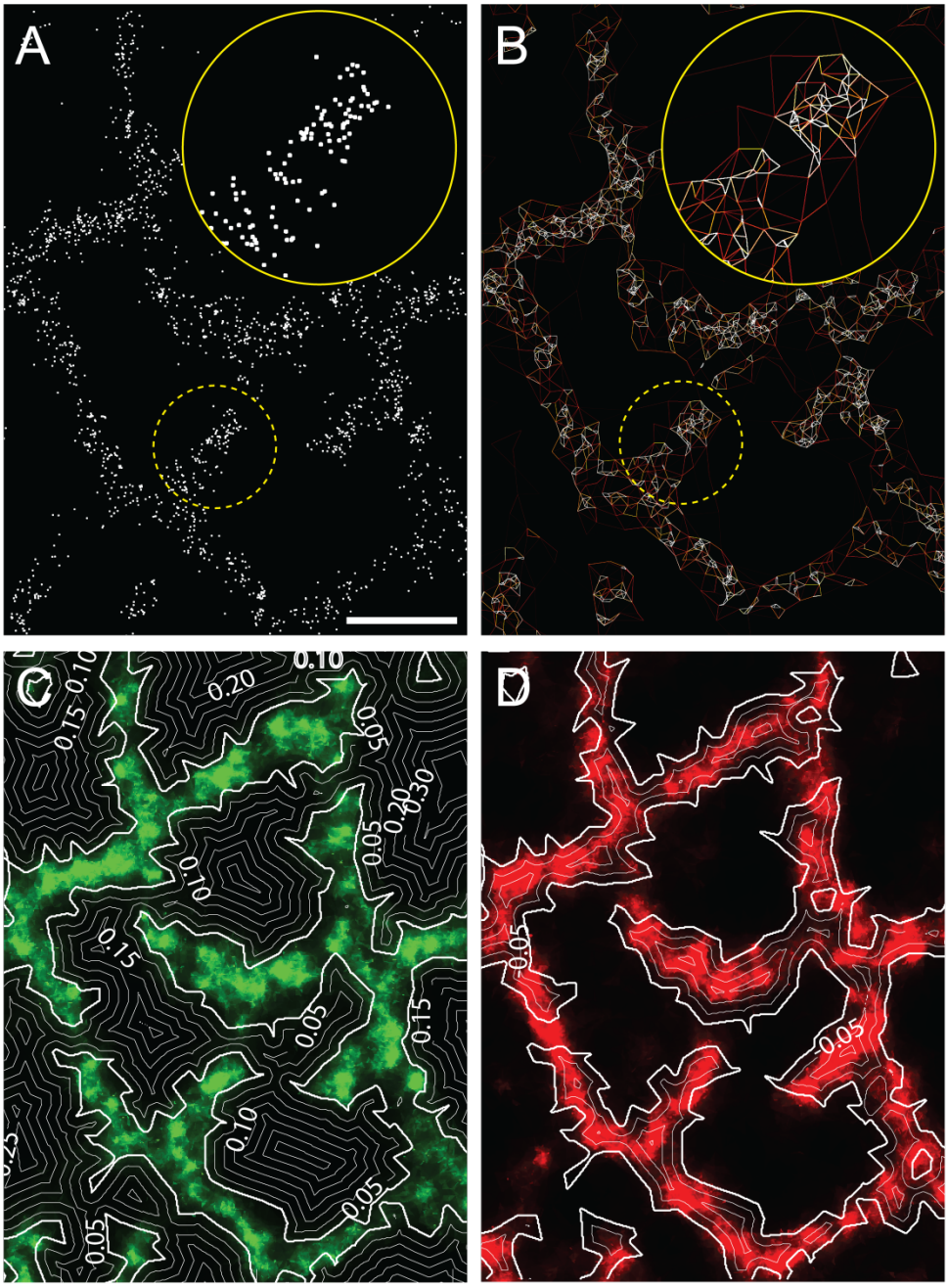

Figure S3: Distance-based analysis of co-localisation. (A) The positions of individual events (each indicated by a white dot) detected over a ~30,000 frame data series of JPH1 labelling within a rat EDL muscle section. (B) Delaunay triangulation between fluorophore positions is calculated and a binary mask is constructed by merging the triangles that are no longer than the effective resolution (30 nm). Insets in A&B indicate magnified view of the region indicated by dashed lines. (C) The binary mask (outlined with the thick white contour) was generated by merging all triangles shorter than 30 nm. This mask used to compute Euclidean distance contours (shown here in 0.05 µm increments) that quantify the distance to the edge of the nearest JPH1 labelled region, here shown overlaid with the greyscale super-resolution image of JPH1 (green). (D) To quantify colocalization these contours were overlaid on the other channel (RyR; here shown in red) and we calculated the fraction of labeling in this channel as a function of this distance to the JPH1 edges. Note that distances within the JPH1

boundaries were counted as negative values. The quantification of fractional labeling into these "distance bands" was used to generate distance histograms. The total co-localizing fraction can be calculated by determining the fraction of labeling with zero or negative distances, i.e. the total fraction within the binary mask. Scale bar: 500 nm.

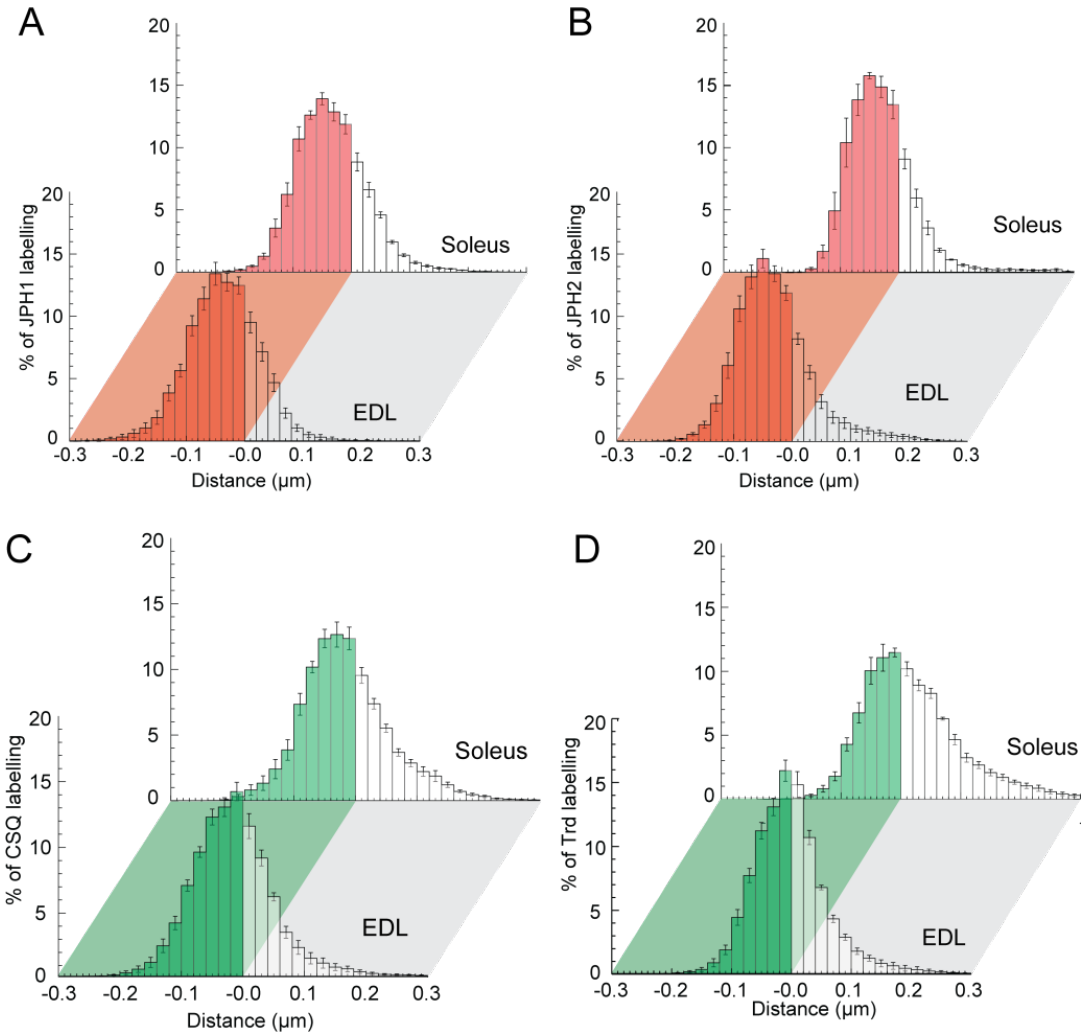

Figure S4: Co-localization analysis comparing the overlap of RyR with JPH1 (A) and JPH2 (B) , JPH1, used as a reporter of RyR cluster arrays, with CSQ (C) and triadin (D) between dSTORM images of EDL and Soleus muscle fibres. The histograms summarise the integrated labelling density of protein-A as a function of the distance to the edge of the binary mask of protein-B.

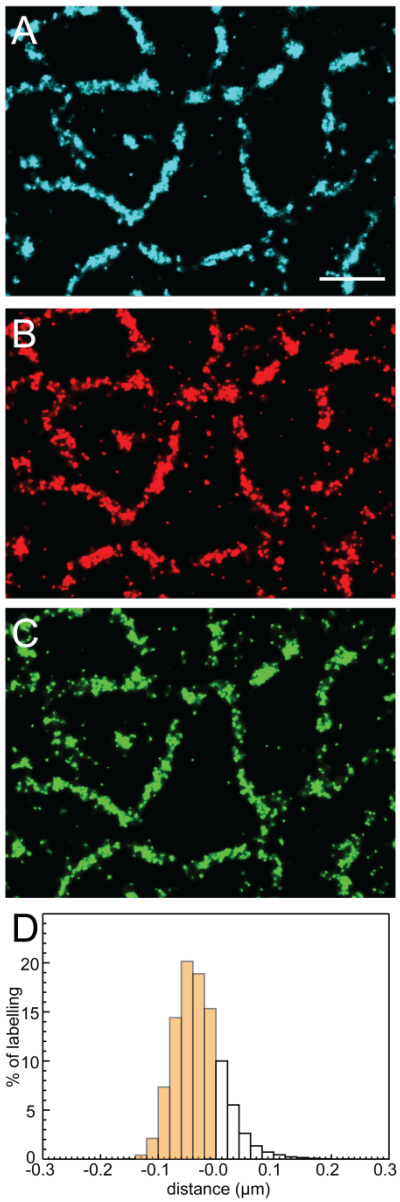

Figure S5: Simulating the effect of the stochastic nature of the antibody labelling of RyR and the detected photoswitching on the measured co-localisation. (A) An experimentally acquired image of RyR staining in a transverse section of rat soleus muscle, which was used to simulate the geometrical constraints of the RyR labelling simulated. Fluorophores staining the triad regions observed in the experimental image were simulated at a density of 0.04 fluorophore/nm^2 and a mean photon count for single molecule events 20-fold higher than that in the background regions. In two independent simulations of the same region, simulated fluorophores were integrated over 10000 frames and the coordinates were rendered into two grey-scale super-resolution images (B & C). (D) The histogram illustrates the percentage of labelling in the first synthetic image as a function of the distance to the nearest edge of labelling in the second image. It was observed that 75-79% of the labelling in a given synthetic image were found in direct overlap with the labelling in an independently simulated image (fraction illustrated by the shaded bars). Scale bar 1 µm.

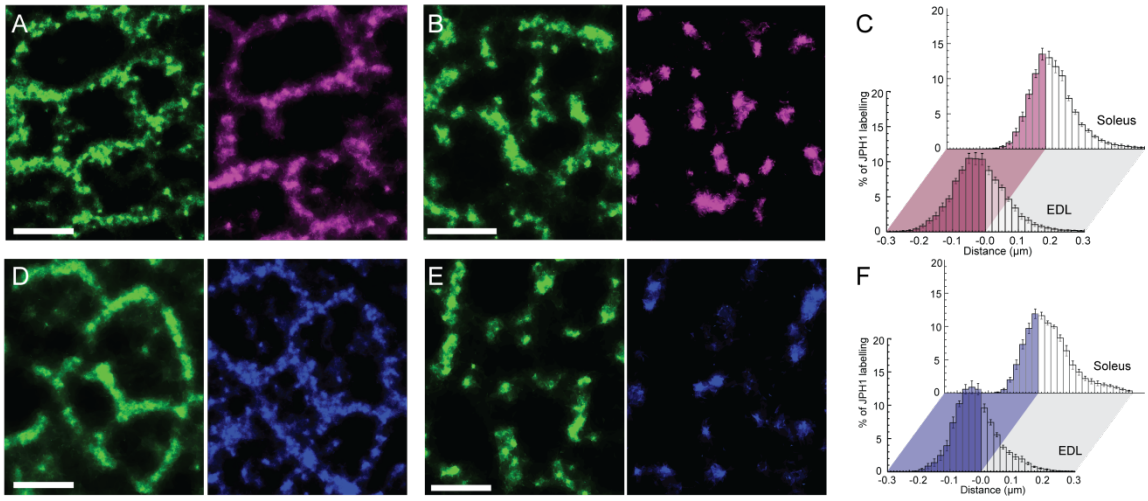

Figure S6. Localisation of CSQ and triadin in relation to triads in fast- and slow-twitch muscle. Transverse dSTORM images contrast relative localisations of JPH1 (green, left) and CSQ (cyan, right) in (A) EDL and (B) SOL fibres. Note the clustered morphology of CSQ in SOL versus the more extended CSQ morphology that better follows the JPH1 staining in EDL. (C) The percentage histograms of JPH1 distribution in relation to the edge of CSQ illustrate the consequently smaller triad area consisting of CSQ in SOL (back) compared to EDL (front). Similar image pairs of JPH1 (green, left) and triadin (blue, right) staining in (D) EDL and (E) SOL fibres indicate a qualitatively similar trend in co-localisation to that between CSQ and JPH1. (F) Percentage histograms JPH1 labelling in EDL (front) and SOL (back) indicate the weak co-localisation of JPH1 with triadin in SOL fibres (shaded area). Scale bars: A, B, D & E: 0.5 µm.

References

1. Tokunaga, M., N. Imamoto, and K. Sakata-Sogawa. 2008. Highly inclined thin illumination enables clear single-molecule imaging in cells. Nature methods 5:159-161.

2. Bossi, M., J. Folling, V. N. Belov, V. P. Boyarskiy, R. Medda, A. Egner, C. Eggeling, A. Schonle, and S. W. Hell. 2008. Multicolor far-field fluorescence nanoscopy through isolated detection of distinct molecular species. Nano letters 8:2463-2468.

3. Baddeley, D., D. Crossman, S. Rossberger, J. E. Cheyne, J. M. Montgomery, I. D. Jayasinghe, C. Cremer, M. B. Cannell, and C. Soeller. 2011. 4D super-resolution microscopy with conventional fluorophores and single wavelength excitation in optically thick cells and tissues. PloS one 6:e20645.

4. Baddeley, D., M. B. Cannell, and C. Soeller. 2010. Visualization of localization microscopy data. Microscopy and microanalysis : the official journal of Microscopy Society of America, Microbeam Analysis Society, Microscopical Society of Canada 16:64-72.

5. Peachey, L. D. and B. R. Eisenberg. 1978. Helicoids in the T system and striations of frog skeletal muscle fibers seen by high voltage electron microscopy. Biophysical journal 22:145-154.

6. Baddeley, D., I. D. Jayasinghe, L. Lam, S. Rossberger, M. B. Cannell, and C. Soeller. 2009. Optical single-channel resolution imaging of the ryanodine receptor distribution in rat cardiac myocytes. Proceedings of the National Academy of Sciences of the United States of America 106:22275-22280.

7. Jayasinghe, I. D., M. B. Cannell, and C. Soeller. 2009. Organization of ryanodine receptors, transverse tubules, and sodium-calcium exchanger in rat myocytes. Biophysical journal 97:2664-2673.

8. Jayasinghe, I. D., D. Baddeley, C. H. Kong, X. H. Wehrens, M. B. Cannell, and C. Soeller. 2012. Nanoscale organization of junctophilin-2 and ryanodine receptors within peripheral couplings of rat ventricular cardiomyocytes. Biophysical journal 102:L19-21.

9. Protasi, F., C. Franzini-Armstrong, and P. D. Allen. 1998. Role of ryanodine receptors in the assembly of calcium release units in skeletal muscle. J Cell Biol 140:831-842.

10. Airey, J. A., C. F. Beck, K. Murakami, S. J. Tanksley, T. J. Deerinck, M. H. Ellisman, and J. L. Sutko. 1990. Identification and localization of two triad junctional foot protein isoforms in mature avian fast twitch skeletal muscle. The Journal of biological chemistry 265:14187-14194.

11. Ohlendieck, K., F. N. Briggs, K. F. Lee, A. W. Wechsler, and K. P. Campbell. 1991. Analysis of excitation-contraction-coupling components in chronically stimulated canine skeletal muscle. European journal of biochemistry / FEBS 202:739-747.

12. Cavagna, M., J. M. O'Donnell, C. Sumbilla, G. Inesi, and M. G. Klein. 2000. Exogenous Ca2+-ATPase isoform effects on Ca2+ transients of embryonic chicken and neonatal rat cardiac myocytes. The Journal of physiology 528 Pt 1:53-63.